J|A|C|S
ARTICLES
Published on Web 06/06/2007

Evolution of Size and Shape in the Colloidal Crystallization of Gold Nanoparticles

Owen C. Compton and Frank E. Osterloh*

Contribution from the Department of Chemistry, University of California, Davis, One Shields Avenue, Davis, California 95161

Received December 17, 2006; E-mail: fosterloh@ucdavis.edu

Abstract: The addition of dodecanethiol to a solution of oleylamine-stabilized gold nanoparticles in chloroform leads to aggregation of nanoparticles and formation of colloidal crystals. Based on results from dynamic light scattering and scanning electron microscopy we identify three different growth mechanisms: direct nanoparticle aggregation, cluster aggregation, and heterogeneous aggregation. These mechanisms produce amorphous, single-crystalline, polycrystalline, and core−shell type clusters. In the latter, gold nanoparticles encapsulate an impurity nucleus. All crystalline structures exhibit fcc or icosahedral packing and are terminated by (100) and (111) planes, which leads to truncated tetrahedral, octahedral, and icosahedral shapes. Importantly, most clusters in this system grow by aggregation of 60−80 nm structurally nonrigid clusters that form in the first 60 s of the experiment. The aggregation mechanism is discussed in terms of classical and other nucleation theories.

Introduction

Periodic arrangement of inorganic particles, or colloidal crystals, continues to be of great academic and technical interest.[1−9] Demonstrated uses for such structures range from porous supports for catalysts[1] and optical band gap materials[5,6] to coatings,[8] chemical sensors,[7] and optically responsive materials.[9] One of the most interesting aspects of colloidal crystals is that their physical properties (optical band gap, magnetism) depend on the crystal lattice parameters and on the crystal morphology.[5,6,9,10] Thus, by controlling these parameters it is possible to create materials with tailored physical properties. Apart from the shape of the building blocks[2,3,11] and their charge,[2] the structure of colloidal crystals is affected by the growth conditions.[11−13] Colloidal crystals can grow either homogeneously or heterogeneously. In homogeneous nucleation, small crystalline regions in a condensing phase form due to structural fluctuations of the colloid. According to classical nucleation theory, the growth of these regions depends on the competition of the chemical potential of the formed nucleus and of its interfacial energy. Growth can only continue when crystals have reached a critical nucleation size, beyond which the increase of interfacial energy is negligible compared to the decrease of chemical potential. The interfacial energy can be substantially lowered in the presence of preformed crystals of the same substance or of particles of a foreign substance (e.g., glass) which serve as sites for aggregation. This is the basis for heterogeneous nucleation.

The mechanism of colloidal crystal nucleation and growth has been studied theoretically[14−17] and experimentally using a range of methods, including confocal microscopy,[18] optical microscopy,[19−21] laser light scattering,[22,23] and electron microscopy.[23−25] These studies have provided estimates for the critical nucleation size, crystal structure, and nucleation rates. However, these investigations have produced little data about the structure and morphology of the intermediates in the early stages of homogeneous crystallization. Particularly for particles in the *sub*-micrometer size regime, there is little known about the beginnings of crystal facet formation, the role of impurities for nucleation, and the mechanism of crystal growth.

(1) Stein, A.; Schroden, R. C. *Curr. Opin. Solid State Mater. Sci.* **2001**, *5* (6), 553−564.
(2) Shevchenko, E. V.; Talapin, D. V.; Kotov, N. A.; O'Brien, S.; Murray, C. B. *Nature* **2006**, *439* (7072), 55−59.
(3) Kitaev, V.; Ozin, G. A. *Adv. Mater.* **2003**, *15* (1), 75-+.
(4) Lu, Y.; Yin, Y. D.; Xia, Y. N. *Adv. Mater.* **2001**, *13* (6), 415−420.
(5) Yablonovitch, E. *J. Phys.: Condens. Matter* **1993**, *5* (16), 2443−2460.
(6) Maldovan, M.; Thomas, E. L. *Nat. Mater.* **2004**, *3* (9), 593−600.
(7) Lee, K.; Asher, S. A. *J. Am. Chem. Soc.* **2000**, *122* (39), 9534−9537.
(8) Jiang, P.; McFarland, M. J. *J. Am. Chem. Soc.* **2004**, *126* (42), 13778−13786.
(9) Fudouzi, H.; Xia, Y. N. *Langmuir* **2003**, *19* (23), 9653−9660.
(10) Sun, S. H.; Murray, C. B.; Weller, D.; Folks, L.; Moser, A. *Science* **2000**, *287* (5460), 1989−1992.
(11) Schaak, R. E.; Cable, R. E.; Leonard, B. M.; Norris, B. C. *Langmuir* **2004**, *20* (17), 7293−7297.
(12) Lee, W.; Chan, A.; Bevan, M. A.; Lewis, J. A.; Braun, P. V. *Langmuir* **2004**, *20* (13), 5262−5270.
(13) Fustin, C. A.; Glasser, G.; Spiess, H. W.; Jonas, U. *Langmuir* **2004**, *20* (21), 9114−9123.
(14) Cacciuto, A.; Auer, S.; Frenkel, D. *Nature* **2004**, *428* (6981), 404−406.
(15) Auer, S.; Frenkel, D. *Nature* **2001**, *409* (6823), 1020−1023.
(16) O'Malley, B.; Snook, I. *Phys. Rev. Lett.* **2003**, *90*, (8).
(17) Sear, R. P. *J. Phys. Chem. B* **2006**, *110* (10), 4985−4989.
(18) Gasser, U.; Weeks, E. R.; Schofield, A.; Pusey, P. N.; Weitz, D. A. *Science* **2001**, *292* (5515), 258−262.
(19) Zhang, K. Q.; Liu, X. Y. *Nature* **2004**, *429* (6993), 739−743.
(20) Wette, P.; Schope, H. J.; Palberg, T. *J. Chem. Phys.* **2005**, *123* (17).
(21) Helseth, L. E.; Wen, H. Z.; Hansen, R. W.; Johansen, T. H.; Heinig, P.; Fischer, T. M. *Langmuir* **2004**, *20* (17), 7323−7332.
(22) Harland, J. L.; vanMegen, W. *Phys. Rev. E* **1997**, *55* (3), 3054−3067.
(23) Lin, X. M.; Wang, G. M.; Sorensen, C. M.; Klabunde, K. J. *J. Phys. Chem. B* **1999**, *103* (26), 5488−5492.
(24) Sigman, M. B.; Saunders, A. E.; Korgel, B. A. *Langmuir* **2004**, *20* (3), 978−983.
(25) Stoeva, S. I.; Prasad, B. L. V.; Uma, S.; Stoimenov, P. K.; Zaikovski, V.; Sorensen, C. M.; Klabunde, K. J. *J. Phys. Chem. B* **2003**, *107* (30), 7441−7448.

Gold nanocrystals are known to form colloidal crystals under a variety of conditions.[23,25−29] Here we investigate the aggregation process using alkylamine-protected gold nanoparticles (21.1 ± 0.7 nm) suspended in chloroform. This system allows us to initiate nanoparticle aggregation with the addition of dodecanethiol and to observe the time-dependent formation of clusters with UV/vis spectroscopy and dynamic light scattering (DLS). We find that the aggregation mechanism for this system differs from classical nucleation theory, in that there is no energetic barrier associated with the aggregation process. All nanoparticles quickly aggregate into a small number of large amorphous clusters and into a majority of small, structurally nonrigid clusters. As these nonrigid clusters aggregate further they produce larger crystalline structures that solidify when reaching sizes between 90 and 200 nm. This aggregation behavior has been theoretically predicted for colloids with short-range interactions.[30,31] We observe crystalline clusters with fcc structures that are terminated by close packed (111) and (100) planes leading to truncated tetrahedral and octahedral shapes. In addition, SEM micrographs provide structural information of core−shell type clusters, in which the nanoparticles grow around an impurity nucleus. The possible model character of these clusters for heterogeneous nucleation is discussed.

Experimental Section

Materials. Tetrachloroauric acid hydrate ($HAuCl_4 \cdot xH_2O$) (99.9% purity) was obtained from Strem Chemicals and stored in a nitrogen atmosphere at −15 °C. Oleylamine (9-octadecenylamine) (80−90% C_{18} content, 97% primary amine content) was obtained from Acros and stored under vacuum over 10 Å molecular sieve pellets. Dodecanethiol (98%+ purity) was used as received from Aldrich. All other chemicals were of reagent grade quality and were purchased from Fischer Scientific and used as received. Samples for SEM analysis were deposited on silicon wafers (Wacker Chemitronic).

Nanoparticle Synthesis. Gold nanoparticles 21.1 ± 0.7 nm in diameter were synthesized using a modified published procedure, by dissolving 100 mg of $HAuCl_4$ in a solution of 2.46 mL of oleylamine and 2.00 mL of toluene.[29] This mixture was added to a refluxing solution of 2.09 mL of oleylamine and 98 mL of toluene and allowed to react for 120 min. Precipitated nanoparticles were collected from the cooled reaction vessel, centrifuged, and washed with a mixture of 19 mL of toluene and 1 mL of oleylamine six times (oleylamine serves to stabilize the dispersion). Nanoparticles were redispersed by dissolving the solid product in a solution of 15 mL of chloroform and 0.50 mL of oleylamine and by sonicating. Samples for further reactions were prepared from this solution by diluting 2 mL in 15 mL of chloroform and 0.50 mL of oleylamine to make a solution with ∼0.20 μmol of gold atom concentration. Ultrasonication was used to fully disperse the product.

Gold Cluster Formation. The formation of gold nanoparticle aggregates was induced by reacting 2 mL of the prepared solution with 28 mg of dodecanethiol. The reaction mixture was then heated to 50 °C for 20 min and was kept in a standard quartz cuvette for the purpose of collecting time-resolved UV/vis spectra. To prepare samples for SEM measurements, the reaction was performed in a 5 mL glass vial, with a silicon wafer at the bottom to collect gold aggregates for imaging with SEM. Samples for DLS measurements were prepared in the same manner; however no silicon wafer was present, and samples were collected by removing 0.25 mL of the reaction solution at the designated times from these vials and quenching aggregation by diluting in 2.5 mL of fresh chloroform.

Instrumentation. UV/vis spectra were collected using an *Ocean Optics, Inc.* DH2000 light source and HR2000 CG-UV-NIR spectrometer. DLS data were collected using a *Microtrac*, Inc. Nanotrac 150. SEM images were collected using an *FEI* XL-30 SFEG SEM. Samples for the SEM were prepared by removing silicon wafers from the reaction vessel of the aggregate synthesis and evaporating the solvent.

Results and Discussion

Monodisperse oleylamine-ligated gold nanoparticles (21.1 ± 0.7 nm) can be synthesized by amine reduction of tetrachloroauric acid in toluene.[29] When dodecanethiol is added to a heated (50 °C) colloidal dispersion of such particles in chloroform, rapid aggregation of gold nanoparticles occurs. This process is initiated by the displacement of the amines by the alkanethiol, due to the greater affinity of sulfur for gold. Because the alkyl group of the thiol is shorter than that of the amine, the thiol-terminated nanoparticles become less soluble in chloroform and start to form clusters. The aggregation is accompanied by a color change from red to purple, and eventually to colorless, as the formed colloidal aggregates sediment from the dispersion (Figure 1A). Sediments can be redispersed in fresh chloroform with only brief ultrasonication to produce solutions with fully restored optical properties (Figure 1B). This shows that the aggregation is reversible. Time-resolved absorption spectra, recorded during aggregation of a nanoparticle sample over a period of 20 min, are shown in Figure 1A. It can be seen that the absorption maximum shifts from an initial value of 528 nm to a final value of 566 nm at 20 min and that the absorption peak undergoes broadening. The change of the absorption maximum with time is also shown in Figure 1C. The most significant optical changes occur during the first 5 min of the experiment, indicating rapid aggregation of gold nanoparticles during this period. The changes in the optical spectra are difficult to interpret quantitatively as they arise from changes in the plasmon band of the aggregating gold nanoparticles[32] and from increased light scattering by Au nanoparticle clusters. In addition, the optical spectra represent an ensemble average of both single and aggregated nanoparticles in the dispersion.

Dynamic light scattering (DLS) provides a more direct measure of the evolution of structures in solution. The temporal evolution of the mean aggregate size is shown in Figure 1D. Initially, before the addition of thiol, DLS measures a mean diameter of 24.5 ± 2.6 nm for the nanoparticle spheres in solution. This diameter is slightly larger than the core diameter from TEM (21.1 ± 0.7 nm), because DLS captures the hydrodynamic diameter, including the ligand shell (∼2.3 nm for oleylamine). Due to cluster formation after addition of thiol, the average diameter of the observed particles in solution increases rapidly to ∼80 nm in the first 200 s. After 650 s into the experiment, the mean particle size approaches 120 nm and no further growth occurs.

Additional information about the evolution of the cluster sizes is contained in Figure 2A. The histogram shows the evolution of sizes versus time with each data point representing an average

(26) Wang, S. H.; Sato, S.; Kimura, K. *Chem. Mater.* **2003**, *15* (12), 2445−2448.
(27) Korgel, B. A.; Zaccheroni, N.; Fitzmaurice, D. *J. Am. Chem. Soc.* **1999**, *121* (14), 3533−3534.
(28) Brown, L. O.; Hutchison, J. E. *J. Phys. Chem. B* **2001**, *105* (37), 8911−8916.
(29) Hiramatsu, H.; Osterloh, F. E. *Chem. Mater.* **2004**, *16* (13), 2509−2511.
(30) Lu, P. J.; Conrad, J. C.; Wyss, H. M.; Schofield, A. B.; Weitz, D. A. *Phys. Rev. Lett.* **2006**, *96* (2).
(31) Charbonneau, P.; Reichman, D. R. *Phys. Rev. E* **2007**, *75* (1).
(32) Quinten, M.; Kreibig, U. *Surf. Sci.* **1986**, *172*, 559−578.

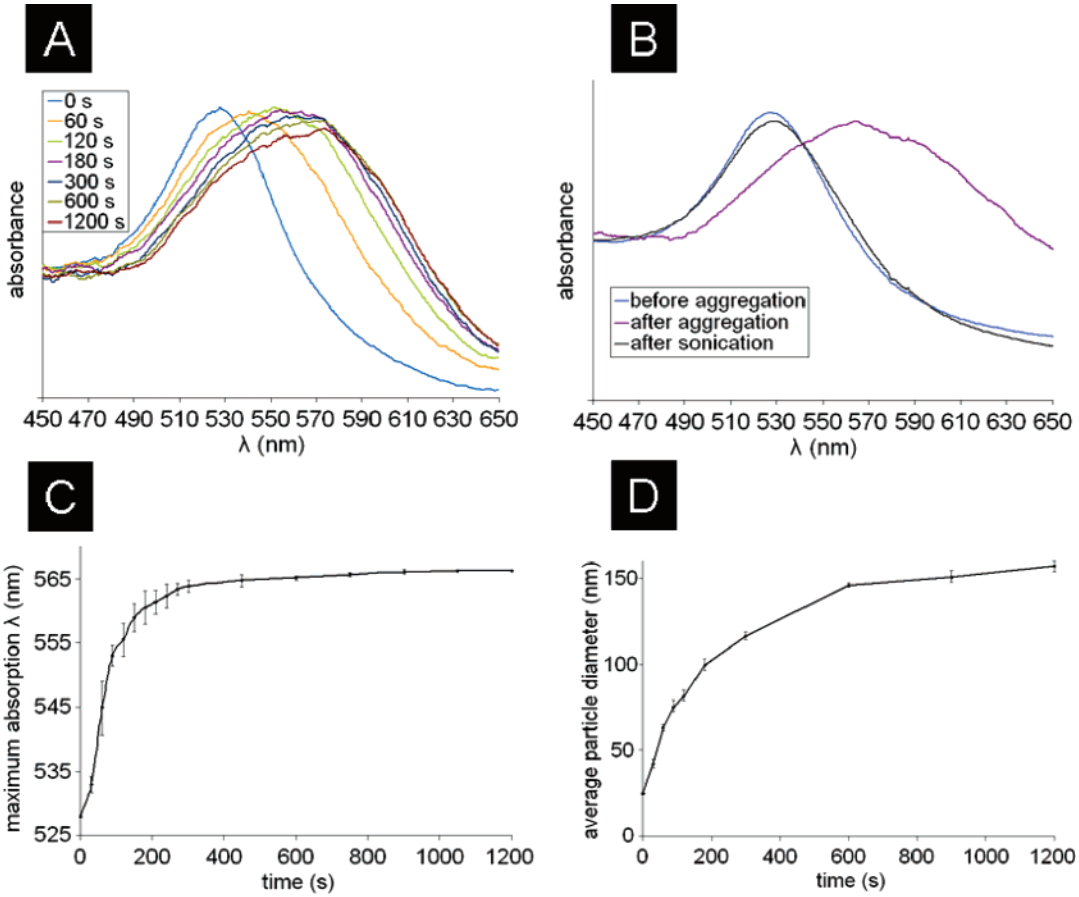

Figure 1. (A) Absorption spectra of oleylamine coated gold nanoparticles in chloroform after addition of dodecanethiol. (B) UV/vis spectra of oleylamine-coated gold particles, dodecanethiol-aggregated nanoparticles, and dodecanethiol-coated particles after ultrasonication (all in chloroform). (C) Plot of the absorption maxima in part A versus time. (D) Plot of the mean diameter of particle aggregates versus time. The standard deviations in parts C and D reflect variations of three separate aggregation experiments.

from three separate aggregation experiments. The data are easiest to analyze in terms of the growth and disappearance of discrete cluster sizes (Figure 2B). Initially, only single 24.5 ± 2.6 nm gold particles are present in the dispersion. Within 60 s of the addition of dodecanethiol, >85% of these particles have aggregated to form mostly clusters of 60−80 nm in diameter, which, based on volume considerations, contain 10−25 nanoparticles. They become the most prominent species in the dispersion at ∼120 s and serve as the main precursor for all other clusters. At 300 s, the fraction of the 60−80 nm clusters has dropped to 10%, and the majority of clusters are 102−122 nm in diameter. Over the remaining time of the experiment these clusters slowly are displaced by clusters of 145−170 nm size.

The data in the histogram clearly show that the majority (∼85%) of nonaggregated gold nanoparticles are consumed in the first 60 s of the experiment. Thus, further growth of clusters can only occur either through aggregation of existing clusters or by particle transfer from one cluster to another. If the latter process was to occur, which corresponds to Ostwald ripening, small clusters would be continuously generated by particle loss. The fact that such small clusters are not observed within the observation limits (10% concentration) of the experimental technique makes this mechanism unlikely.

A growth model based on cluster aggregation reactions is supported by simple theoretical considerations. Calculations based on first-order consecutive aggregation reactions (eq 1−3) show that the growth data shown in Figure 2B can be approximated with a set of four differential equations with separate rate constants k_{1-3} (full details on page S-2 in the Supporting Information). Here each cluster species forms by symmetrical aggregation of smaller clusters, e.g.,

$$1 + 1 \xrightarrow{k_1} 2 \qquad 2 + 2 \xrightarrow{k_2} 4 \qquad 4 + 4 \xrightarrow{k_3} 8 \quad \text{(eqs. 1–3)}$$

For simplicity, the model is terminated at the octamer, and back-reactions, which expectedly would be slow at the beginning of the aggregation experiment, are neglected. The results of this model, with 2.14×10^{14} as the initial number of gold nanoparticles in the colloidal gold solution and $k_1 = 0.1\ s^{-1}$, are shown in Figure 2C. It can be seen that the main features of the experimental data in Figure 2B, the fast decay of single particles, the temporary maxima of dimers and tetramers, and the sigmoidal shape of the time trace for the octamers, can be reproduced satisfactorily. Given the simplicity of the model the rate constants k_2 and k_3 cannot be determined with any confidence; however, to satisfactorily fit the curves for the dimers and tetramers, it is required that k_2 be at least three times greater than k_3. A decrease of the rate constants is in agreement with the expectation that larger clusters experience higher activation barriers for aggregation than smaller clusters. Larger clusters are more rigid than small ones, making "sticky collisions" more difficult.

While the majority of clusters follow these growth trends, the histogram in Figure 2A also shows a fraction of large gold

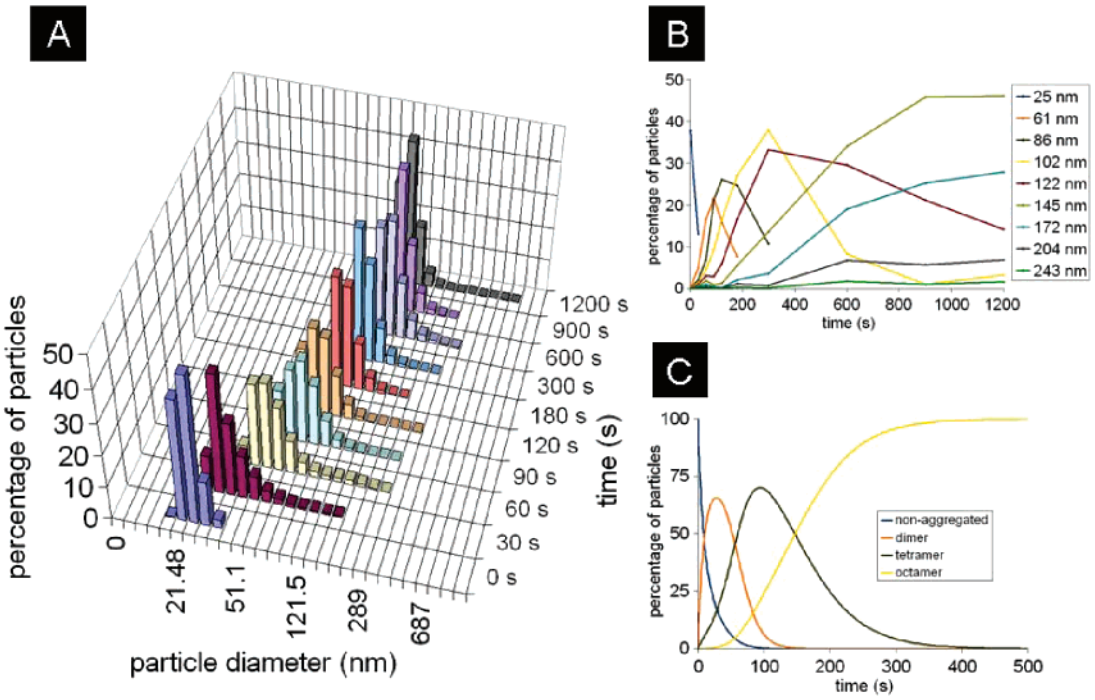

Figure 2. (A) Size dispersion data collected via DLS. Each data point represents the average of three separate experiments. (B) Time dependent evolution of aggregate size. Due to instrument limitations, small <10% cluster populations cannot be observed. (C) Simulation of aggregation based on first-order kinetics.

clusters with sizes of 150−290 nm that appears within 30 s of the beginning of the experiment. The fraction of these "early" clusters is small (5.6%) and remains nearly constant over the duration of the experiment. This significantly shorter time scale for the formation of the clusters suggests a difference in growth mechanism. These clusters seem to grow from direct aggregation of gold nanoparticles and not from other clusters. The time-dependent evolution of these clusters cannot be determined as it depends on the unknown number of nucleation sites in the initial solution. However, if one assumes that these clusters grow by first-order kinetics, the rate constant for this aggregation process should simply be given by $k_1 = 0.1$ (eq 1).

Structures and shapes of clusters were observed with scanning electron microscopy. Appropriate samples were obtained by placing a silicon wafer in the reaction mixture, onto which clusters were deposited by sedimentation. This sample collection method preferentially captures the larger, denser clusters. SEM observations showed that approximately 30% of the collected clusters were amorphous, roughly 50% were polycrystalline, and the remaining 20% were single crystalline. Examples of amorphous aggregates are shown in Figure 3A (for high resolution images see Supporting Information). With sizes up to 2 μm, these clusters are among the largest species in the sample. Round or ellipsoidal shapes were frequent, with small (∼100 nm) domains on the surface showing order, but lacking the facets characteristic of crystals. The shape and the lack of long-range order suggest that these clusters did grow over very short time scales under diffusion-limited conditions from a dispersion supersaturated with thiol-coated nanoparticles. Thus these objects can be identified as belonging to the "early" cluster fraction that formed within the first 30 s of the aggregation experiment. A possible explanation for the formation of these amorphous clusters comes from a recent Gibbs ensemble Monte Carlo calculation.[31] For colloids with short-range interactions between the particles, such calculations predict the formation of amorphous particle agglomerates that subsequently transform into colloidal crystals. In this context the appearance of ordered regions on the aggregate surface can be seen as the beginning of a transformation from a glass into a crystal. However, this crystallization process seems to be too slow to compete with the fast deposition of nanoparticle material on the aggregate surface.

Single-crystalline clusters are shown in Figure 3B. These clusters reach sizes between 200 and 450 nm, and all exhibit face centered cubic packing (fcc) of gold nanoparticles. All of these clusters are terminated by (111) and (100) surfaces leading to truncated tetrahedral and hexagonal shapes. The clusters in Figure 3B are presented in order of increasing size. A possible growth mechanism involves the raspberry-shaped cluster on the left as precursor. Based on volume considerations, this cluster contains approximately 50 gold nanoparticles. The spherical shape suggests that these particles are arranged as hexagonal close packed shells around a nucleus in the center. Further growth transforms the cluster into the truncated tetrahedral shape next to it, which contains ∼400 gold nanoparticles. Continued growth along [111] and [100] directions increases the cluster size, until the cluster precipitates from the dispersion and continues to grow heterogeneously on the bottom of the reaction flask. Because access to the cluster is blocked at the bottom, growth only continues at the sides and on the top, transforming the truncated tetrahedral morphology into the hexagonal plate shape.

Polycrystalline clusters are observed in a variety of sizes ranging from 200 nm to over 2 μm (Figure 3C). Quite common among the smaller examples are icosahedral and decahedral shapes that are terminated by (111) planes. These shapes correspond to multiply twinned crystals with icosahedral shell packing (at distance far from the center, the packing ap-

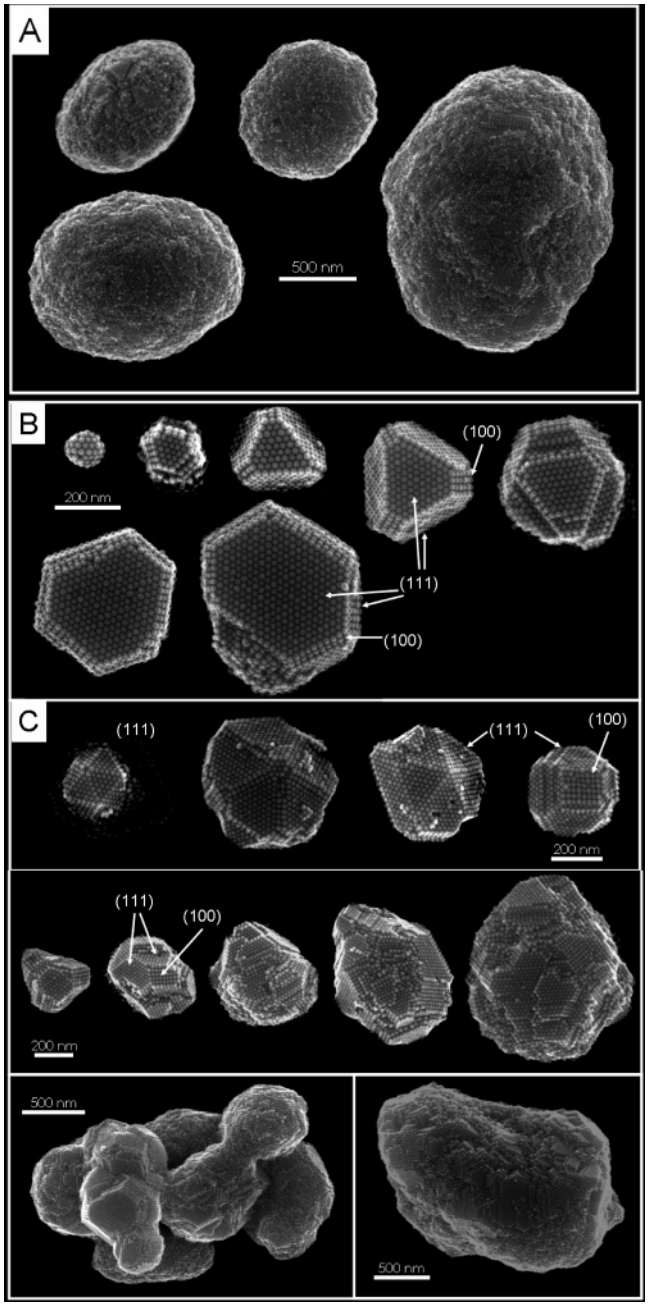

Figure 3. (A) Amorphous gold nanoparticle clusters. (B) Single crystalline clusters. (C) Polycrystalline clusters.

proximates fcc packing).[33] A similar crystal morphology has been observed for nickel and gold nanoparticles.[34,35] The cluster on the far right exhibits the shape of a truncated octahedron. This cluster exhibits the fcc structure type and is terminated by (111) and (100) planes. Based on the SEM data, one cannot differentiate between a single crystalline or polycrystalline structure for these clusters.

The larger clusters in Figure 3C are made of 200−400 nm large domains of an fcc lattice with distinct facets that mostly represent 111 and 100 planes. In principle, these domains could have formed either through incorporation of growth defects or as a result of random aggregation of smaller clusters. The latter mechanism seems likely for some of the larger clusters, whose "peanut" shapes suggest buildup from two smaller clusters.

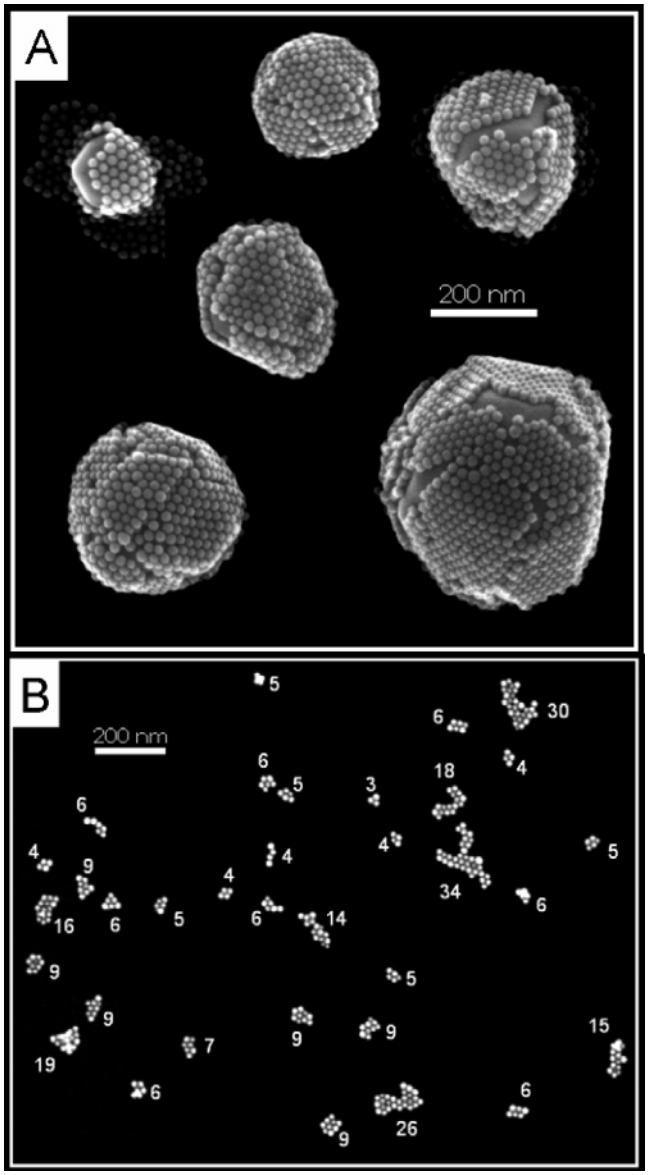

Figure 4. (A) Core−shell type gold nanoparticle clusters. (B) Gold nanoparticle clusters remaining in liquid phase after 20 min.

A small percentage of the observed clusters have the core−shell type morphology shown in Figure 4A. The center of these clusters is made of impurity particles (probably silica) that were present in a very small quantity (<0.001%) in the reaction mixture. Despite their irregular shapes, these impurities are surrounded by well ordered arrangements of closely packed gold nanoparticles. Most of the gold particles are organized into monolayers, but double layers are also present. In these cases the beginning of the formation of lattices with well formed facets is evident. Some surface areas of the impurity particles are bare, suggesting that detachment of the monolayer has occurred in these regions. It is notable that these bare areas mostly coincide with regions of high curvature of the central particle. Apparently gold nanoparticles stick less tightly to these regions.

For molecular and ionic crystals it is well-known that impurities can serve as nucleation sites.[36] For colloidal crystals this function is less established. However, a recent theoretical

(33) MacKay, A. L. *Acta Crystallogr.* **1962**, *15*, 916−918.
(34) Kim, F.; Connor, S.; Song, H.; Kuykendall, T.; Yang, P. D. *Angew. Chem., Int. Ed.* **2004**, *43* (28), 3673−3677.
(35) Gillet, M. F.; Brieu, M. *Z. Phys. D: At., Mol. Clusters* **1989**, *12* (1−4), 107−111.

study suggested that when the size of the impurity is less than 10 times larger than the nanoparticles, the impurity will be incorporated into the colloidal crystal as it grows.[14] If the impurity is larger it will not be incorporated and instead functions as a catalyst, with colloidal crystals growing on the impurity's face until detachment occurs. For the present system the clusters shown in Figure 4A do not have a catalytic function, as the data suggest that nanoparticle aggregation into small clusters occurs quickly and without an energy barrier.

Finally, SEM is able to identify one additional type of nanoparticle cluster. Samples taken from the reaction mixture after 20 min reveal small clusters containing 3−34 nanoparticles (Figure 4B). Due to their small size, these clusters remain dispersed in the solvent at the end of the aggregation experiment. All observed clusters are flat against the surface of the silicon substrate, suggesting weak interactions between the nanoparticles and structural nonrigidity. In solution, these clusters likely form spherical structures with diameters of 40−90 nm, based on close packing. We believe that these clusters correspond to the 60−80 nm cluster group that constitutes the major solution species in the first 30−120 s of the experiment (see above). Aggregation of these "liquid" clusters produces solid clusters with mostly fcc structures. Based on the sizes of the liquid clusters (Figure 4B, 90 nm, ∼35 nanoparticles) and the smallest crystalline ones (Figure 3B, 200 nm, ∼400 nanoparticles), the transition from a nonrigid to a rigid cluster occurs between 90 and 200 nm (∼35 to 400 nanoparticles). Incidentally, this value is similar to experimental and theoretical values for the critical nucleation size in classical nucleation theory.[15,18]

Conclusion

In summary this study provides the first detailed look at the size and shape evolution of the intermediates in the reactive crystallization of sub-100 nm gold nanoparticles. We are able to identify three different growth mechanisms: direct nanoparticle aggregation, cluster aggregation, and heterogeneous aggregation. These mechanisms produce amorphous, single-crystalline, polycrystalline, and core−shell type clusters. The crystalline structures mostly belong to the fcc structure type, and their morphology is defined by (111) and (100) planes. Importantly, we find that the growth mechanism in this system is different from classical nucleation theory, in that there is no critical nucleation size for crystal growth. Instead, most of the nanoparticles aggregate into structurally nonrigid (liquid) cluster intermediates, which serve as the building blocks for further growth. The structures become solid as they reach sizes of 35−200 nanoparticles. Our observations are interesting in light of recent Gibbs ensemble Monte Carlo calculations on a colloid with short-range interactions.[31] Theoretically, such a colloid is found to undergo a two-step nucleation process starting with the initial formation of disordered nanoparticle clusters followed by the formation of an ordered phase. This two-step mechanism leads to a lowering free energy pathway and faster crystal growth compared to classical nucleation theory. The calculations further predict that crystallization takes place via cluster condensation, and not by aggregation of individual nanoparticles. This agrees well with what we have observed for the present system of thiolate-stabilized gold nanoparticles.

Acknowledgment. This work was supported by the National Science Foundation (CTS-0427418). We thank Suwimon Ariyaprakai of the Department of Food Science and Technology at UC Davis for assistance with the DLS instrument.

Supporting Information Available: Differential rate equations for the evolution of nanoparticle cluster sizes and high resolution versions of Figures 3 and 4. This material is available free of charge via the Internet at http://pubs.acs.org.

JA069033Q

(36) Fletcher, N. H. *J. Chem. Phys.* **1958**, *29*, 572−576.